

Assessing the Hazard Posed by Ryugu Ejecta Dynamics on Hayabusa2 Spacecraft

By Stefania Soldini¹⁾ and Yuichi Tsuda¹⁾

¹⁾ *Institute of Space and Astronautical Science/JAXA, Sagamihara, Japan*
(Received 31st March, 2017)

This paper investigates the hazard posed by the asteroid ejecta dynamics to Hayabusa2 spacecraft. Past studies concluded that the regions around Ryugu are expected to be cleared after two weeks from the impact event if size particles of 1 mm are considered. However, Ryugu asteroid is composed by regolith (highly porous) material with high likelihood of ejecta in 1 cm size. Natural impact phenomena on asteroids observed from Rosetta spacecraft suggest that dust particles of 1 cm size in diameter can be captured for several months in orbit around the asteroid. This condition is extremely dangerous for Hayabusa2 spacecraft as a collision with small particles can severely damage the spacecraft structure and compromise its functionality. The fate of the asteroid ejecta is here investigated through numerical modelling. A high fidelity dynamical model is used where the asteroids gravity harmonics, its ephemeris, spin rotation and inclination, the solar radiation pressure perturbation and the effect of the Sun third-body perturbation are taken into account.

Key Words: Fate of Ejecta, Perturbed Two-Body Problem, 1:1 Resonances and Dynamical Substitutes

1. Introduction

Hayabusa2 mission is the Japanese sample and return mission to Ryugu asteroid launched in 2014. It is the successor mission to JAXA's Hayabusa mission to Itokawa asteroid. Hayabusa2 spacecraft will encounter Ryugu in June 2018, followed by the asteroid touch-down mission phase in the first half of 2019. The challenge that Hayabusa2 spacecraft will encounter is the asteroid cratering mission phase [12]. During the asteroid proximity operations, Hayabusa 2 spacecraft is set to a base position, Home Position (HP), at 20 km above the asteroid facing the sub-Earth direction. This technique was successfully used by Hayabusa mission and it is known as hovering¹. All operations such as trajectory conjunction manoeuvre, gravity measurement and fly-around observation, cratering and touch down start from HP and return to HP position after each mission operation [12].

Hayabusa2 spacecraft is equipped with a Small Carry on Impactor (SCI), and it is expected to create a crater of 2-3 m size to allow the sampling of substrate asteroid materials [7]. The SCI is a compact kinetic impactor released along the HP axis at 500 km from the asteroid surface to create an artificial crater on it. As part of Hayabusa 2 experiment, the spacecraft will release a camera to observe the impact event while the mother spacecraft will fly away from HP position to be placed in a safe location from the asteroid dust ejecta. An impact velocity of 2 km/s is required for Hayabusa 2 mission for creating a few meters size crater [7].

Previous work in JAXA showed that the asteroid ejecta will leave the landing site after two weeks, therefore allowing Hayabusa 2 mother spacecraft to return safely at HP and continue with the scheduled mission operations [4]. However, the debris trail of asteroid P/2010 A2 observed by Rosetta spacecraft suggests that those debris are the result of a natural collision event occurred with the asteroid in 2009 [11]. Therefore, dust particles of diameter size larger than 1 mm can last in as-

teroid orbits for several months or years. Ryugu asteroid is a C-type asteroid composed of regolith material with large scale size particles on the order of cm in the diameter size. Those large-size particles pose a great risk for Hayabusa 2 spacecraft [5]. This paper investigates the hazard posed by the asteroid ejecta dynamics to Hayabusa2 spacecraft. The fate of the asteroid ejecta is here investigated through numerical modelling for diameter-size dust particles of 0.01, 0.1, 1 and 1 cm. A high fidelity dynamical model is used where the asteroids gravity harmonics, its ephemeris, spin rotation and inclination, the solar radiation pressure perturbation and the effect of the Sun third-body perturbation are taken into account. This is done to observe with numerical experiment if the ejecta can naturally follow long-term stable orbits that can preclude the spacecraft to touchdown the asteroid surface for collecting samples. Together with the numerical experiments, the dynamics close to the asteroid 1:1 resonance are here explored under the solar radiation pressure effect to show numerical evidence of the presence of dynamical substitutes (stable orbits) for Ryugu asteroid when the system is no longer autonomous [2, 14]. The dust ejecta is also displayed in the Hill reference frame to verify if with our set of initial conditions dust particles can be trapped in terminator orbits [8].

The paper is organised as follows: Section 2. shows the reference systems used for this analysis. The dynamics of the perturbed two-body problem in the rotating frame are given in Section 3., where the dynamics around the 1:1 resonances is explored in Section 4.. Section 5. presents the dynamics in the perturbed two-body problem in the inertial coordinates. Finally, the fate of the ejecta dynamics around Ryugu asteroid is discussed in Section 6.

2. Reference Frames and Rotations

Hayabusa 2 spacecraft will operate around Ryugu asteroid at an hovering point of 20 km from the surface (Home Posi-

¹The spacecraft does not orbit the asteroid.

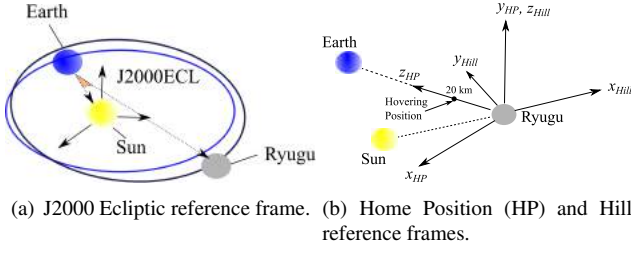


Fig. 1: Reference systems for Haybusa 2 mission.

tion). The Home Position (HP) reference frame, shown in Figure 1(b), is a special reference system for Haybusa 2 mission where the z -axis is along the Earth-asteroid distance, the Sun-Asteroid distance belongs to the positive x and z coordinates (HP). Thus:

- The z -axis is defined by: $\hat{r}_3 = \frac{\mathbf{r}_{Earth}}{|\mathbf{r}_{Earth}|}$;
- The y -axis is defined by: $\hat{r}_2 = \frac{\mathbf{r}_{Earth} \times \mathbf{r}_{Sun}}{|\mathbf{r}_{Earth} \times \mathbf{r}_{Sun}|}$;
- The x -axis is defined by:

$$\hat{r}_1 = \frac{\left(\frac{\mathbf{r}_{Earth} \times \mathbf{r}_{Sun}}{|\mathbf{r}_{Earth} \times \mathbf{r}_{Sun}|} \right) \times \left(\frac{\mathbf{r}_{Earth}}{|\mathbf{r}_{Earth}|} \right)}{\left| \left(\frac{\mathbf{r}_{Earth} \times \mathbf{r}_{Sun}}{|\mathbf{r}_{Earth} \times \mathbf{r}_{Sun}|} \right) \times \left(\frac{\mathbf{r}_{Earth}}{|\mathbf{r}_{Earth}|} \right) \right|}$$

Note that $\mathbf{r}_{Earth} = \mathbf{r}_{Earth}|_{(J2000ECL)} - \mathbf{r}_A|_{(J2000ECL)}$ and $\mathbf{r}_{Sun} = -\mathbf{r}_{Sun}|_{(J2000ECL)}$. As shown in Figure 1(a), the J2000ECL is the inertial reference frame centred at the Sun where the ephemeris of the planets (DE430 model) and Ryugu (2162173 model) are given with respect to the ecliptic². The HP frame is used to describe the Small Carry on Impactor (SCI) dynamics and for the definition of the ejecta initial state (launching site and speed from the asteroid surface). In our analysis, the J2000ECL is convenient for downloading the ephemeris data; however, when performing rotation between different system, a reference frame centred at the asteroid is preferable. Therefore, we introduce the Asteroid-Centered Ecliptic (ACE) frame that is a translation from J2000ECL to J2000ECL centred at the Asteroid.

The transformation from HP frame to ACE frame is given by:

$$\mathbf{r}_{ACE} = \mathbf{R}_{HP} \cdot \mathbf{r}_{HP}, \quad (1)$$

with

$$\mathbf{R}_{HP} = [\hat{r}_1 | \hat{r}_2 | \hat{r}_3]. \quad (2)$$

For the velocities, we have:

$$\mathbf{v}_{ACE} = \mathbf{R}_{HP} \cdot \mathbf{v}_{HP} + \dot{\mathbf{R}}_{HP} \cdot \mathbf{r}_{HP}, \quad (3)$$

and

$$\dot{\mathbf{R}}_{HP} = [\dot{\hat{r}}_1 | \dot{\hat{r}}_2 | \dot{\hat{r}}_3], \quad (4)$$

with

- $\dot{\hat{r}}_3 = \frac{\mathbf{v}_{Earth}}{|\mathbf{r}_{Earth}|} - \frac{(\mathbf{r}_{Earth} \bullet \mathbf{v}_{Earth})}{|\mathbf{r}_{Earth}|} \frac{\mathbf{r}_{Earth}}{|\mathbf{r}_{Earth}|^2}$;
- $\dot{\hat{r}}_2 = \frac{\mathbf{v}_{Earth} \times \mathbf{r}_{Sun}}{|\mathbf{r}_{Earth} \times \mathbf{r}_{Sun}|} + \frac{\mathbf{r}_{Earth} \times \mathbf{v}_{Sun}}{|\mathbf{r}_{Earth} \times \mathbf{r}_{Sun}|} - \frac{\mathbf{r}_{Earth} \times \mathbf{r}_{Sun}}{|\mathbf{r}_{Earth} \times \mathbf{r}_{Sun}|^2} \cdot \left(\frac{(\mathbf{r}_{Earth} \times \mathbf{r}_{Sun}) \bullet ((\mathbf{v}_{Earth} \times \mathbf{r}_{Sun}) + (\mathbf{r}_{Earth} \times \mathbf{v}_{Sun}))}{|\mathbf{r}_{Earth} \times \mathbf{r}_{Sun}|} \right)$

²The ephemeris of the planets are given from the NASA-JPL Spice Toolkit MICE for Matlab.

$$\dot{\hat{r}}_1 = (\dot{\hat{r}}_2 \times \hat{r}_3) + (\hat{r}_2 \times \dot{\hat{r}}_3)$$

As the dynamics of the ejecta are given in an asteroid centred frame, we introduce two additional reference frame: the Asteroid-Centered Inertial (ACI) frame and the Asteroid-Centered Asteroid Fixed (ACAF) frame (rotating frame with angular velocity equal to the asteroid spin ratio). In first approximation, the Ryugu gravity model selected is the triaxial-ellipsoid. The gravity harmonics are expressed in the ACAF frame, while the dynamics are given in both ACI and ACAF frame. The dynamics expressed in the ACAF frame with only gravity harmonics give rise of 1:1 resonances, where two stable equilibrium exist for Ryugu asteroid. This may suggest that the asteroid ejecta could be trapped in those stable region for several days, thus dynamics around those points have to be further explore.

The simplest rotation takes into account of the sidereal motion (spin-axis rotation) of the asteroid:

- $\mathbf{r}_{ACAF} = \mathbf{T}(t) \cdot \mathbf{r}_{ACI}$
- $\mathbf{v}_{ACAF} = \mathbf{T}(t) \cdot \mathbf{v}_{ACI} + \dot{\mathbf{T}}(t) \cdot \mathbf{r}_{ACI}$
- $\mathbf{a}_{ACAF} = \mathbf{T}(t) \cdot \mathbf{a}_{ACI} + 2\dot{\mathbf{T}}(t) \cdot \mathbf{v}_{ACI} + \ddot{\mathbf{T}}(t) \cdot \mathbf{r}_{ACI}$

where

$$\mathbf{T}(t) = \begin{bmatrix} \cos \phi & \sin \phi & 0 \\ -\sin \phi & \cos \phi & 0 \\ 0 & 0 & 1 \end{bmatrix}, \quad (5)$$

with $\phi = \omega_a t + \phi_0$ and ω_a is the Ryugu asteroid spin ratio. Table 1 shows Ryugu asteroid properties where $\omega_a = 2\pi/(T \cdot 3600)$ rad/s. Note that $\dot{\mathbf{T}}(t) = -[\boldsymbol{\omega} \times] \mathbf{T}(t)$ and $\boldsymbol{\omega} = [0, 0, \omega_a]^T$ with:

$$[\boldsymbol{\omega} \times] = \begin{bmatrix} 0 & -\omega_a & 0 \\ \omega_a & 0 & 0 \\ 0 & 0 & 0 \end{bmatrix} \quad (6)$$

while $\ddot{\mathbf{T}}(t) = -[\boldsymbol{\omega} \times] \dot{\mathbf{T}}(t)$. The inverse rotation is given by:

- $\mathbf{r}_{ACI} = \mathbf{T}'(t) \cdot \mathbf{r}_{ACAF}$
- $\mathbf{v}_{ACI} = \mathbf{T}'(t) \cdot (\mathbf{v}_{ACAF} - \dot{\mathbf{T}}(t) \cdot \mathbf{r}_{ACI})$
- $\mathbf{a}_{ACI} = \mathbf{T}'(t) \cdot (\mathbf{a}_{ACAF} - 2\dot{\mathbf{T}}(t) \cdot \mathbf{v}_{ACI} - \ddot{\mathbf{T}}(t) \cdot \mathbf{r}_{ACI})$

Among the possible stable orbits that exist around a small body, terminator orbits are polar Sun-synchronous orbit that have been proven to be particularly stable under the effect of perturbations [8]. In our analysis, the results will be shown in the Hill reference frame (Figure 1(b)) to check if our set of initial conditions for the ejecta can lead to dust particles naturally trapped in terminator orbits. Therefore, the Hill frame is defined as follow. First, the position of Ryugu is given with respect to the Sun. The reference system of Hill is centred at the asteroid and the Sun is in the negative x coordinates:

- $\hat{\mathbf{c}}_1 = \frac{\mathbf{r}_a}{|\mathbf{r}_a|}$;
- $\hat{\mathbf{c}}_3 = \frac{\mathbf{h}}{|\mathbf{h}|} = \frac{\mathbf{r}_a \times \mathbf{v}_a}{|\mathbf{r}_a \times \mathbf{v}_a|}$;
- $\hat{\mathbf{c}}_2 = \frac{\hat{\mathbf{c}}_3 \times \hat{\mathbf{c}}_1}{|\hat{\mathbf{c}}_3 \times \hat{\mathbf{c}}_1|}$,

where \mathbf{r}_a and \mathbf{v}_a are the position and the velocity of the asteroid with respect to the Sun (J2000ECL frame). The transformation from the Hill to the ACE frame is given by:

$$\mathbf{r}_{ACE} = \mathbf{C} \cdot \mathbf{r}_{Hill}. \quad (7)$$

with

$$\mathbf{C} = [\hat{\mathbf{c}}_1 | \hat{\mathbf{c}}_2 | \hat{\mathbf{c}}_3]. \quad (8)$$

and the velocity is

$$\mathbf{v}_{ACE} = \mathbf{C} \cdot \mathbf{v}_{Hill} + \dot{\mathbf{C}} \cdot \mathbf{r}_{Hill}, \quad (9)$$

with

$$\dot{\mathbf{C}} = [\dot{\hat{\mathbf{c}}}_1 | \dot{\hat{\mathbf{c}}}_2 | \dot{\hat{\mathbf{c}}}_3], \quad (10)$$

where

$$\bullet \dot{\hat{\mathbf{c}}}_1 = \frac{\mathbf{v}_a}{|\mathbf{r}_a|} - \frac{(\mathbf{r}_a \bullet \mathbf{v}_a)}{|\mathbf{r}_a|} \frac{\mathbf{r}_a}{|\mathbf{r}_a|^2},$$

$$\bullet \dot{\hat{\mathbf{c}}}_3 = \frac{\mathbf{r}_a \times \mathbf{a}_a}{|\mathbf{r}_a \times \mathbf{v}_a|} - \left[\hat{\mathbf{c}}_3 \bullet \frac{\mathbf{r}_a \times \mathbf{a}_a}{|\mathbf{r}_a \times \mathbf{v}_a|} \right] \frac{\hat{\mathbf{c}}_3}{|\mathbf{r}_a \times \mathbf{v}_a|},$$

where \mathbf{a}_a is the acceleration of the asteroid that can be approximated numerically³.

$$\bullet \dot{\hat{\mathbf{c}}}_2 = (\dot{\hat{\mathbf{c}}}_3 \times \hat{\mathbf{c}}_1) + (\hat{\mathbf{c}}_3 \times \dot{\hat{\mathbf{c}}}_1).$$

In our analysis, we want to verify that the landing site is cleared from dust particles within two weeks to meet the mission constrains. Therefore, the objective of this paper is not to study long term orbit evolution and the maximum simulation time considered is of 30 days. Within this time span, the Sun-Asteroid and the Earth-Asteroid distance shift of few degrees by keeping those distances constant. Thus, our work does not lose of generality by considering the matrices \mathbf{R}_{HP} and \mathbf{C} constant over the time span and consequently, we set their derivatives to zero in Eq. (4) and Eq. (10) respectively. As the impact phase is scheduled for June 2019, we choose the 1st of June 2019 as reference epoch to download the ephemeris of the planets and asteroid.

| Property | Value |
|---|---|
| Pole orientation ($\lambda_{ecl}, \beta_{ecl}$) | (329°, -39°) |
| Rotation period (T) | 7.631 [h] |
| JD ₀ | 2454289 |
| ϕ_0 | 0° |
| Effective radius (r_a) | 440 [m] |
| Ellipsoidal shape | a = 446.5 [m] b = 439.7 [m] c = 433.9 [m] |
| μ_a | 32 [m ³ /s ²] |
| Density (ρ_a) | 1270 [kg/m ³] |
| Orbital period (T_o) | 1.3 [years] |

Table 1: Ryugu asteroid physical properties.

The dynamics of the ejecta is subject to environmental perturbations as the asteroid's irregular shape and spin ratio, the

³Note that Spice Toolkit does not provide the accelerations of the planets.

solar gravity and solar radiation pressure. Depending on the altitude of the ejecta, some perturbations are more dominant than others. It is possible to define the following sphere around the asteroid [15]:

- The Hill sphere (solar tides equals the asteroid gravity):

$$R_1 = r_m \left(\frac{\mu_a}{\mu_{Sun}} \right)^{1/3} = 110.8 \quad [km] \quad (11)$$

- The sphere of influence (the asteroid gravity is dominant):

$$R_2 = r_m \left(\frac{\mu_a}{\mu_{Sun}} \right)^{2/5} = 6.3 \quad [km] \quad (12)$$

- The solar gravity equals the asteroid gravity:

$$R_3 = r_m \left(\frac{\mu_a}{\mu_{Sun}} \right)^{1/2} = 87.4 \quad [m] \quad (13)$$

where $r_m = \sqrt[3]{\frac{T_o^2 \mu_{Sun}}{4\pi^2}}$ (mean radius, Ryugu in a circular orbit around the Sun). T_o is the orbital period (Table 1) and $r_m = 1.78 \cdot 10^8$ [km].

3. Dynamics in the Rotating (ACAF) Reference Frame

The equations of motion in the close vicinity of the asteroid are given in the two-body problem with the gravity harmonics expressed in the rotating (ACAF) frame, where the spin axis is aligned with the z -axis [9]:

$$\begin{aligned} \ddot{x} - 2\omega_a \dot{y} &= -\frac{\mu_a}{r^3} x + \omega_a^2 x + a_{px}, \\ \ddot{y} + 2\omega_a \dot{x} &= -\frac{\mu_a}{r^3} y + \omega_a^2 y + a_{py}, \\ \ddot{z} &= -\frac{\mu_a}{r^3} z + a_{pz}, \end{aligned} \quad (14)$$

with a_{px} , a_{py} and a_{pz} are the components of the perturbation acceleration \mathbf{a}_p :

$$\mathbf{a}_p = \mathbf{a}_g + \mathbf{a}_{srp}. \quad (15)$$

The gravity perturbation term \mathbf{a}_g is given by $\{B_x, B_y, B_z\}$. B is the potential associated to the asteroid harmonics defined as [13]⁴:

$$B(r, \phi, \lambda) = -\frac{\mu_{sb}}{r} \left\{ \sum_{n=1}^{\infty} \left(\frac{r_{sb}}{r} \right)^n \left[\sum_{m=1}^n P_{nm}(\sin \phi) [C_{nm} \cos(m\lambda) + S_{nm} \sin(m\lambda)] \right] \right\}, \quad (16)$$

where n and m are respectively the order and the degree of the harmonics taken into account; r , ϕ (latitude) and λ (longitude) are the coordinates of the dust in spherical coordinates with respect to the ACAF frame; P_{nm} are the Legendre polynomial; while C_{nm} and S_{nm} are the Stockes coefficients. For a triaxial ellipsoid, the Stocks coefficient are defined as [10]:

⁴Eq. (16) is numerically quite slow. We replace recursive functions with for loops to speed up the code. Moreover, a C code file generated from Matlab Coder has been used to overcome the running time speed issue of Matlab when using for loops.

- $C_{20} = \frac{1}{5R^2} \left(c^2 - \frac{a^2+b^2}{2} \right)$,
- $C_{22} = \frac{1}{20R^2} (a^2 - b^2)$,
- $C_{40} = \frac{15}{7} (C_{20}^2 + 2C_{22}^2)$,
- $C_{42} = \frac{5}{7} C_{20} C_{22}$,
- $C_{44} = \frac{5}{28} C_{22}^2$,

and their values are listed in Table 2 for Ryugu asteroid.

Note that B is expressed in spherical coordinates (r, ϕ, λ) , while the accelerations in Eq.(14) are expressed in Cartesian ACAF coordinates (x, y, z) . Thus, a transformation from spherical to Cartesian coordinates is required [13]:

$$\begin{Bmatrix} B_x \\ B_y \\ B_z \end{Bmatrix} = \begin{bmatrix} \frac{x}{r} & -\frac{xz}{(r^2\sqrt{x^2+y^2})} & -\frac{y}{(x^2+y^2)} \\ \frac{y}{r} & -\frac{yz}{(r^2\sqrt{x^2+y^2})} & \frac{x}{(x^2+y^2)} \\ \frac{z}{r} & \frac{\sqrt{x^2+y^2}}{r^2} & 0 \end{bmatrix} \begin{Bmatrix} B_r \\ B_\phi \\ B_\lambda \end{Bmatrix} \quad (17)$$

| $C_{n,m}$ | Value |
|-----------|--------------------|
| C_{20} | -0.008346943756564 |
| C_{22} | 0.001556320160869 |
| C_{40} | 0.000159676574917 |
| C_{42} | -0.000009278940607 |
| C_{44} | 0.000001513832777 |

Table 2: Ryugu Stockes coefficients.

The solar radiation pressure perturbation (a_{srp}) for dust particles is given by [9]:

$$\mathbf{a}_{srp} = -(1 + \rho)P_0 \frac{A}{m} \frac{(\mathbf{d} - \mathbf{r})}{|\mathbf{d} - \mathbf{r}|^3}, \quad (18)$$

where \mathbf{d} and \mathbf{r} are the distances of the Sun and of the dust from the asteroid respectively. The Sun pressure, P_0 is $10^8 \text{ kg km}^3 \text{ s}^{-2} \text{ m}^{-2}$, the reflectivity coefficient for the dust, ρ , is assumed equal to 1 (worst case), and A and m are the area and the mass of a spherical dust particles. In Table 3, four different dust size particles have been used to compute the sphere radius. Above those radius, solar radiation pressure is dominant with respect to the asteroid gravity.

| Particle Diameter | Sphere Radius |
|-------------------|---------------|
| 0.1 mm | 440 [m] |
| 1 mm | 1.03 [km] |
| 1 cm | 3.25 [km] |
| 0.1 m | 10.28 [km] |

Table 3: Solar radiation pressure sphere of influence.

The values of those spherical radius have been found as in Ref [15] from Figure 2. Figure 2 shows the normalised solar tide (solid black line) and the SRP (dash line) scaled by the Ryugu gravity. The picture is given in logarithmic scale and the unitary horizontal line (dash dot line) represents the case in which the perturbation equals the gravity of the asteroid. The

intersection between the dashed lines and the solid line with the unitary horizontal line gives the value of the radius of influence of the considered perturbation. The four radius of influence for four size particle are summarised in Table 3, while the intersection between the solid line and the horizontal line represent the Hill sphere (R_1) that was previously computed as in Eq. (11).

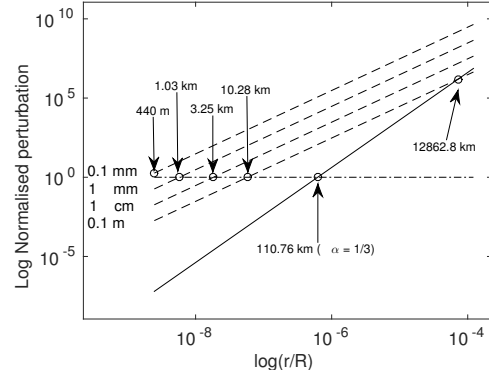


Fig. 2: Solar radiation pressure (dashed lines) for four particle diameters (0.1 mm, 1 mm, 1 cm and 0.1 m) and solar tides (black line) scaled with the Ryugu gravity force. This picture was done following Ref [15]

When the effect of SRP is neglected ($\mathbf{a}_{srp} = \mathbf{0}$ in Eq. (15)), the energy of the system is given by:

$$E = \frac{1}{2}(\dot{x}^2 + \dot{y}^2 + \dot{z}^2) - \frac{1}{2}\omega_a^2(x^2 + y^2) - \frac{\mu a}{r} - B. \quad (19)$$

Fig. 3 shows the shape of the potential energy (when the velocity in Eq.(19) is equal to zero) as a function of r and λ for $\phi = 0^\circ$ (i.e. at the equator).

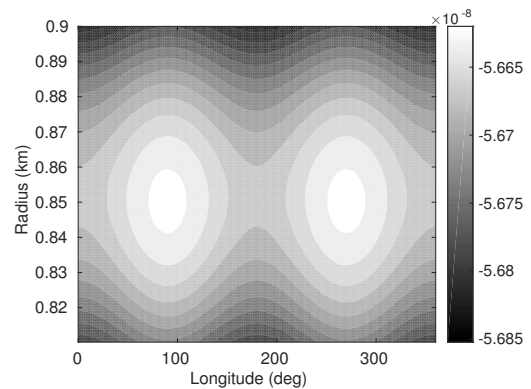


Fig. 3: Potential Energy as function of r and λ for $\phi = 0^\circ$.

Notice that Eq.(14) is an autonomous system when the SRP effect is neglected that admits four equilibrium points (1:1 resonances between the asteroids spin rate and the equatorial orbit around the asteroid) [6]. For a triaxial ellipsoid, the four equilibrium points lie on the equator ($\phi = 0^\circ$) and are located at λ equal to $0^\circ, 90^\circ, 180^\circ$ and 270° [10]. The equilibrium point can be found by imposing the velocities and accelerations equal to zero in Eq.(14) (for $\mathbf{a}_{srp} = \mathbf{0}$). The coordinates of the equilibrium points are shown in Fig. 4 where the saddle points have

coordinate $(\pm 852, 0, 0)$ km, while the center points have coordinate $(\pm 850.3, 0, 0)$ km.

As for the Hill problem, the Zero Velocity Curves (ZVC) of the perturbed two-body problem (also known as Roche Lobe [9]) give qualitative information on the dust particles motion. We recall that, if the energy of the dust is less than the energy of the saddle points, then the ZVC separate the inner from the outer motion. In this case, the motion around the asteroid will be confined if the dust is inside this region. On the other hand, when the energy of the dust increases, a gap close to the saddle is opened, connecting the inner and outer regions. In this case the trajectory of the dust can escape. For the point mass model, the escape velocity is given as:

$$v_f = \sqrt{\frac{2\mu a}{r_a}} = 0.38 \text{ [m/s]}. \quad (20)$$

The escape velocity approximated in Eq. (20) is an overestimation of the real escape velocity as escape trajectories are possible when the energy of the dust is above the energy of the saddle and this occur for velocities lower than the one computed in Eq. (20).

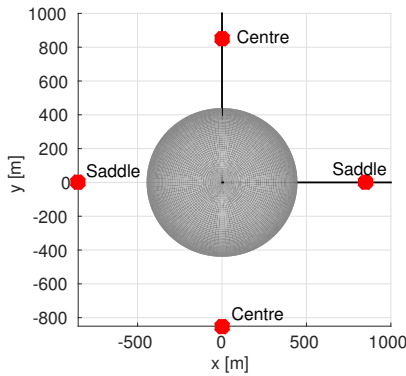
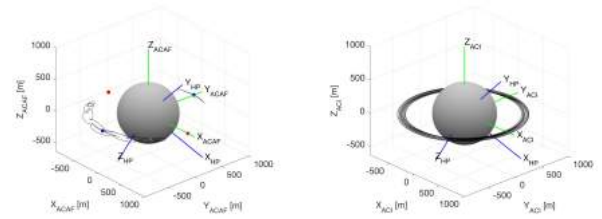


Fig. 4: Equilibrium points for Ryugu modelled as a triaxial ellipsoid.

4. Ejecta dynamics around the center equilibrium under the effect of SRP perturbation

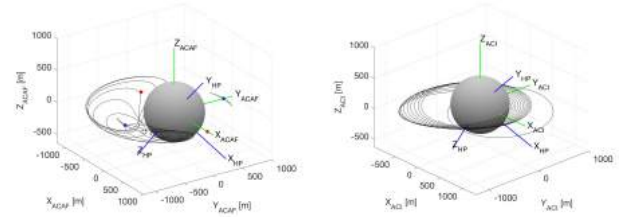
In this section, the dynamics behaviour of small size particles around a center equilibrium are investigated in the ACAF dynamics as in Ref [1]. Eq. (14) is an autonomous system when the effect of SRP is neglected, thus stable trajectories arise close to the center as shown in Figure 5. In Figure 5, an initial condition close to the center with $y = -840.34$ m, $v_x = -0.001$ m/s and $x = z = v_y = v_z = 0$ m was integrated for 5 days and a stable solution around the center arises where a particle in those trajectory can last for more than 30 days. Note that, in Ref [1] the SRP effect was not taken into account and similar trajectories have been found as in Figure 5.

When the effect of SRP is taken into account, Eq. (14) is no longer an autonomous system due to the time dependence of the SRP term. Therefore, the equation of the energy (Eq. (19)) no longer holds and also the existence of the equilibrium points is not straight forward. Previous work regarding the perturbed Re-

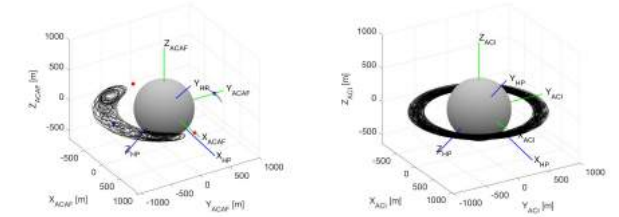


(a) Trajectory in the ACAF frame. (b) Trajectory in the ACI frame.

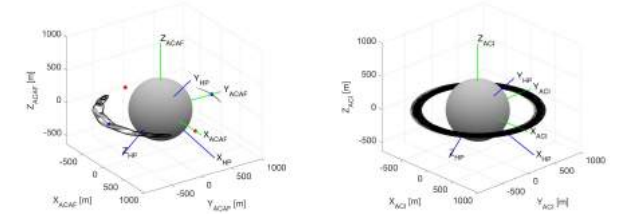
Fig. 5: Dust dynamics around a center equilibrium when the effect of SRP perturbation is neglected. 5 days of simulation time.



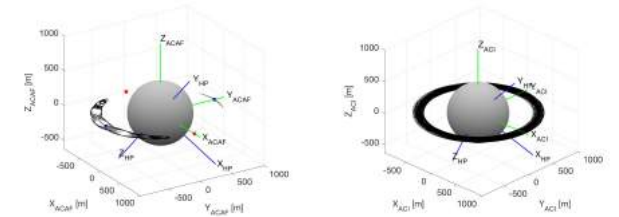
(a) $d = 0.01$ cm (ACAF frame). (b) $d = 0.01$ cm (ACI frame).



(c) $d = 0.1$ cm (ACAF frame). (d) $d = 0.1$ cm (ACI frame).



(e) $d = 1$ cm (ACAF frame). (f) $d = 1$ cm (ACI frame).



(g) $d = 10$ cm (ACAF frame). (h) $d = 10$ cm (ACI frame).

Fig. 6: Dust dynamics around a center equilibrium under the effect of SRP perturbation. For $d = 0.1, 1$ and 10 cm the simulation time is 30 days while for $d = 0.01$ cm the impact trajectory last for 23 days

stricted Three Body Problem (R3BP) show that under the effect of perturbations the R3BP is no longer an autonomous system and it gives rise of what is known as dynamical substitutes [2]. The dynamical substitutes are stable orbit around the equilib-

rium points for the autonomous system (no SRP) that under the effect of periodic perturbations replace the former equilibrium points with a stable orbit. Recent work has been carried out for the perturbed two body problem with SRP effect for asteroid applications where the dynamical substitute have been found [14].

Figure 6 shows a numerical experiment where the dynamics of the dust particles is computed under the SRP perturbation effect. Four dust particles diameter have been considered as 0.01, 0.1, 1 and 10 cm size. As one can see, there is numerical evidence that for particles of diameter size major than 0.1 cm a stable solution arises around the previous center point suggesting the presence of a dynamical substitute as shown in Figures 6(c)-6(h). Conversely, diameter size lower than 0.01 cm brakes the stability region showing an unstable impact trajectory in Figures 6(a)-6(b). Although, diameter less than 0.01 cm shows that can clear the region around the asteroid due to the effect of SRP, the time of flight before impact can be long with respect to the mission constraints as for Figures 6(a)-6(b) where the time of flight of the dust is 23 days.

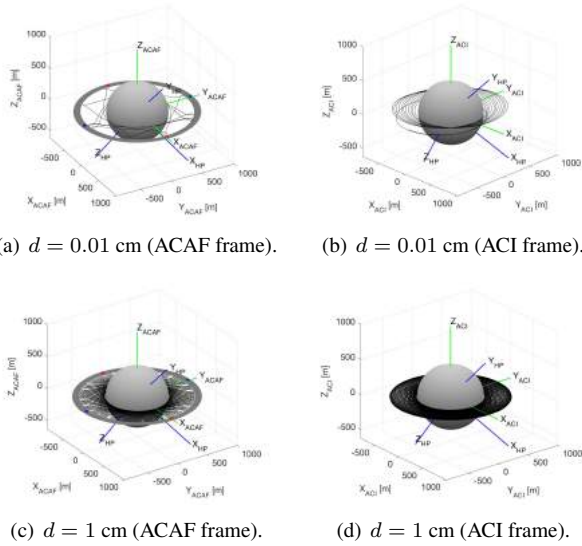


Fig. 7: Dust dynamics around a center equilibrium under the effect of SRP perturbation. For $d = 1$ cm the simulation time is 30 days while for $d = 0.01$ cm the impact trajectory last for 3 days

Figure 7 shows the dynamics of dust particle size of 0.01 and 1 cm in diameter for an initial condition with $y = -796$ m, $v_x = -0.001$ m/s and $x = z = v_y = v_z = 0$ m (closer to the asteroid surface). The gray area in Figures 7(a) and 7(c) correspond to the forbidden region when SRP is not taken into account, however the dynamics are given under the effect of the SRP perturbation. The dynamics with only gravity gives rise of a bounded motion around the asteroid that can last for more then 30 days. Again, dust particles with diameter size lower than 0.01 cm tent to have an impact trajectory while higher diameter can lead to a long term dynamics on the order of months. Therefore, further studies need to be carried out around those stable regions when the shape model of the asteroid is used in replacement of the triaxial ellipsoid approximation.

5. Dynamics in the Inertial (ACI) Reference Frame

The equations of motion of the perturbed two-body problem expressed in the ACI reference frame are given by:

$$\begin{aligned}\ddot{x} &= -\frac{\mu_a}{r^3}x + a_{px} \\ \ddot{y} &= -\frac{\mu_a}{r^3}y + a_{py} \\ \ddot{z} &= -\frac{\mu_a}{r^3}z + a_{pz}\end{aligned}\quad (21)$$

For simplicity, we kept the same notation for both the inertial (ACI) and rotating (ACAF) coordinates. The perturbation acceleration expressed in the ACI coordinates is:

$$\mathbf{a}_p = \mathbf{a}_g + \mathbf{a}_{SRP} + \mathbf{a}_s. \quad (22)$$

where we considered as before the gravity harmonics, \mathbf{a}_g in Eq. (17), and the solar radiation pressure effect, \mathbf{a}_{SRP} in Eq. (18). In this case, we also add the third body perturbation of the Sun, \mathbf{a}_s [9]:

$$\mathbf{a}_s = -\mu_s \left(\frac{\Delta}{|\Delta|^3} - \frac{\mathbf{r}}{r^3} \right), \quad (23)$$

with μ_s the Sun mass parameter, Δ the distance between the Sun and the dust particles and r the distance of the dust particles with the asteroid. Figure 8 shows the planets third body (Figure 8(a)) and tides (Figure 8(b)) perturbations during Hayabusa2 mission operations. As one can see, the Sun is the major perturbation with respect to the other planets. Therefore, our numerical analysis includes the Sun perturbations.

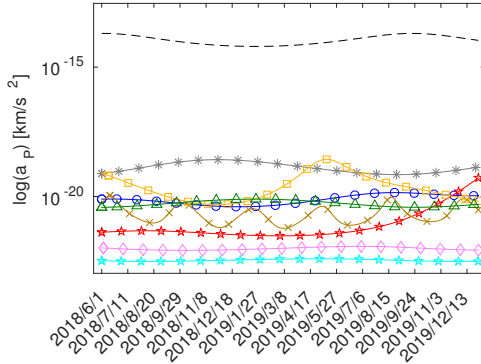
6. Fate of the Ejecta after the SCI impact

In this section, the evolution of the ejecta after the SCI impact is investigated. At first, we identify the uncertainties in the impact point knowing that the nominal altitude of the mother spacecraft, h , is of 510 m before the SCI is released along the z -axis of the HP reference frame. We then integrate the equations of motion, shown in Eq. (21), to find the possible impact points of the SCI as a function of the initial uncertainties of the mother spacecraft. For each impact point, we modelled the crater formation by using empirical laws in order to have an initial set of launching speed of the ejecta and crater size.

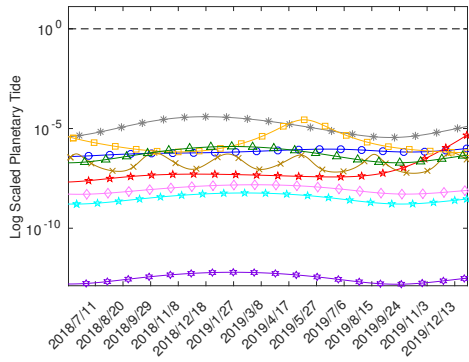
Once the initial condition for the ejecta is set, Eq. (21) is integrated over 30 days and the trajectory evolution of the ejecta is then shown in the ACI, ACAF and Hill reference frames. This is done to check if with this set of initial conditions, dust particles can stay in orbit around the asteroid for long time. The same study is done for four different size of dust particles of 0.01, 0.1, 1, and 10 cm. A total of 51 impacts are considered (included the nominal case) and for each impact 1000 solutions have been sampled along the crater (100 along the crater radius and 100 along the angle that span the entire crater perimeter). Therefore, a total of 51000 simulations have been run for each size particles with a total of 204000 solutions investigated.

6.1. Uncertainties in the SCI impact

Starting from the paper of Saiki et al [7], we considered the uncorrelated covariance matrix for both the mother spacecraft and the SCI separation manoeuvre uncertainties. The mean vec-



(a) Third body perturbation.



(b) Planetary tides scaled with the Sun tides.

Fig. 8: Logarithmic scale of the third body perturbation and tides. Legend: Sun (black dashed line), Earth (blue circles), Mars (red stars), Jupiter (gray asterisks), Mercury (brown crosses), Venus (yellow squares), Saturn (green triangles), Uranus (pink diamonds), Neptune (light blue stars) and Pluto (violet hexagams). These plots have been found similar from Ref [15].

tor of the mother spacecraft position (μ_p) and velocity (μ_v) are respectively:

$$\mu_p = \begin{bmatrix} 0 \\ 0 \\ h + r_a \end{bmatrix} \quad \mu_v = \begin{bmatrix} 0 \\ 0 \\ v_z \end{bmatrix}, \quad (24)$$

where h is the already mentioned mother spacecraft altitude and r_a is the asteroid radius shown in Table 1. v_z is 0.15 m/s. The uncorrelated covariance matrices in position and velocity are:

$$Cov_p = \begin{bmatrix} \sigma_x^2 & 0 & 0 \\ 0 & \sigma_y^2 & 0 \\ 0 & 0 & \sigma_z^2 \end{bmatrix} \quad Cov_v = \begin{bmatrix} \sigma_{v_x}^2 & 0 & 0 \\ 0 & \sigma_{v_y}^2 & 0 \\ 0 & 0 & \sigma_{v_z}^2 \end{bmatrix}, \quad (25)$$

with 3σ defined as follow [7]:

- $3\sigma_x = 3\sigma_y = 50$ m
- $3\sigma_z = 30$ m
- $3\sigma_{v_x} = 3\sigma_{v_y} = 2$ cm/s
- $3\sigma_{v_z} = 3$ cm/s

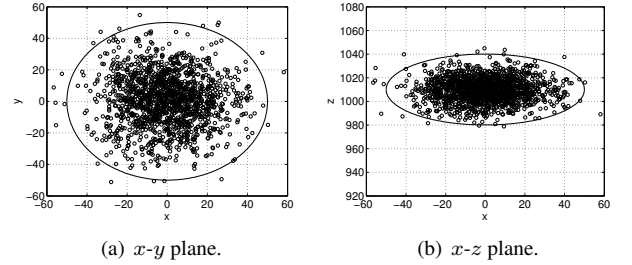
For the SCI uncertainty manoeuvre, we have:

$$\mu_{vm} = \begin{bmatrix} 0 \\ 0 \\ v_{zm} \end{bmatrix} \quad Cov_{vm} = \begin{bmatrix} \sigma_{v_{xm}}^2 & 0 & 0 \\ 0 & \sigma_{v_{ym}}^2 & 0 \\ 0 & 0 & \sigma_{v_{zm}}^2 \end{bmatrix}, \quad (26)$$

with $v_{zm} = 205$ mm/s, $3\sigma_{v_{xm}} = 3\sigma_{v_{ym}} = 20$ mm/s and $3\sigma_{v_{zm}} = 5$ mm/s [7]. As the mother spacecraft and the SCI separation uncertainties are uncorrelated (independent random variables), we can write:

$$\mu_{vt} = \mu_v + \mu_{vm} \quad Cov_{vt} = Cov_v + Cov_{vm}. \quad (27)$$

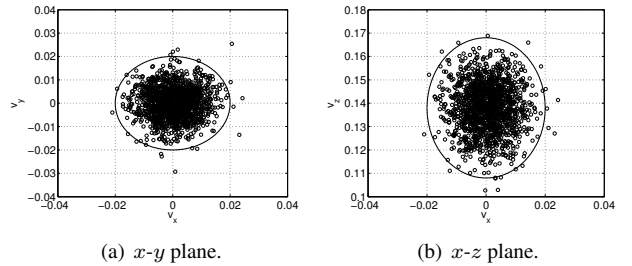
Figure 9 shows the uncertainties in position of the mother spacecraft, while Figure 10 shows the mother spacecraft uncertainties in velocity. The uncertainties contribution of both the mother spacecraft and the SCI are shown in Figure 11.



(a) x - y plane.

(b) x - z plane.

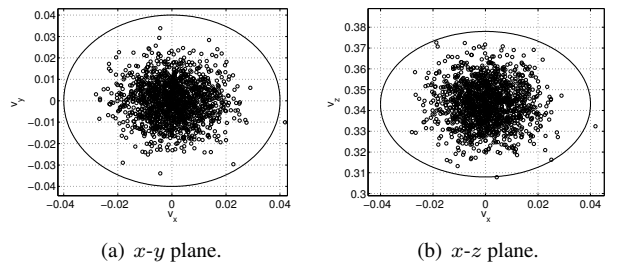
Fig. 9: Error of the mother spacecraft in position (HP reference frame).



(a) x - y plane.

(b) x - z plane.

Fig. 10: Error of the mother spacecraft in velocity (HP reference frame).



(a) x - y plane.

(b) x - z plane.

Fig. 11: Error of the mother spacecraft and the SCI separation manoeuvre in velocity (HP reference frame).

Figure 12 shows the 51 impact points selected as initial state

for the crater model as a function of the mother spacecraft and the SCI manoeuvre uncertainties. The red star represents the reference impact points.

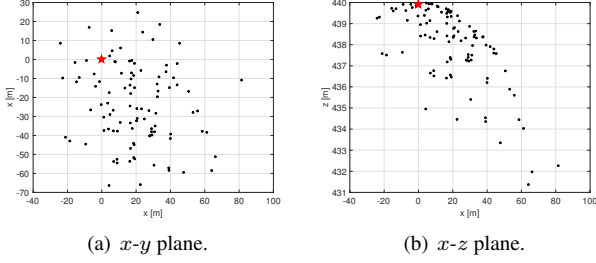


Fig. 12: Impact points of the SCI in the HP reference frame.

6.2. Initialisation State of the Ejecta

The crater size and particles launch speed is given through the ejecta scale laws that are empirical laws found from experimental study [3].

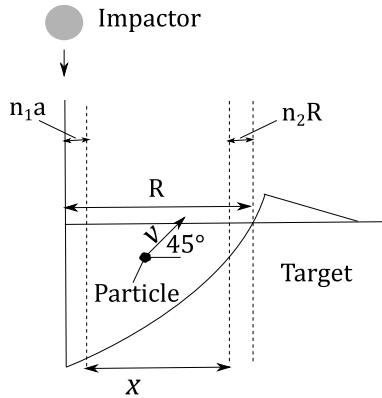


Fig. 13: Crater model [3].

The empirical law for the crater radius is [3]:

$$R = K_1 \left[\frac{ga}{U^2} \left(\frac{\rho_a}{\delta} \right)^{\frac{2\nu}{\mu}} + \left(\frac{Y}{\rho U^2} \right)^{\frac{(2+\mu)}{2}} \left(\frac{\rho_a}{\delta} \right)^{\frac{\nu(2+\mu)}{\mu}} \right]^{-\frac{\mu}{(2+\mu)}}; \quad (28)$$

and the empirical law of the launching speed is [3]:

$$v = UC_1 \left[\frac{x}{a} \left(\frac{\rho_a}{\delta} \right)^{\nu} \right]^{-\frac{1}{\mu}} \left(1 - \frac{x}{n_2 R} \right)^p \text{ with } n_1 a \leq x \leq n_2 R \quad (29)$$

where, g is the gravity constant of Ryugu (μ_a/r_a^2 in Table 1), a is the projectile radius, U is the velocity of the projectile, ρ_a is the density of the target (Ryugu asteroid in Table 1), δ is the density of the projectile, R is the crater radius (shown in Figure 13) and Y the target strength. n_1 , n_2 , ν , μ , p , C_1 and K_1 are non-dimensional parameters depending on the material properties of the projectile and the target. Tables 4-5 show the values for the regolith material coefficients [3] and of the impactor [7]. The x coordinate is where the material is ejected from the crater as there is no particles ejected from the impact point and on the crater border. Using the parameter of tables 4-5, the radius, R ,

is equal of 2.3 m. In this model, the ejecta is launched at 45° with respect to the asteroid surface. Along the x coordinate, we sampled the first 100 points from the center of the crater as shown in Figure 14 (black asterisks). This is done as for ejecta launch speed way below the escape velocity the dust dynamics is dominated by the gravity of the asteroid; therefore it will re-impact the surface. Other 100 points are then considered to cover the asteroid entire perimeter with a total of 1000 points for each impact. The impact position was given in the HP reference frame while here are expressed in the ACI reference frame. The model of the crater holds for each of the 51 impacts considered in our uncertainty analysis. The center of the crater will be therefore shifted in the ACI reference frame depending on the initial impact point of the SCI.

| Property | Value |
|----------|-------|
| n_1 | 1.2 |
| n_2 | 1 |
| C_1 | 0.18 |
| ν | 0.4 |
| μ | 0.46 |
| p | 0.3 |
| K_1 | 0.725 |
| Y | 1 |

Table 4: Highly porous material (regolith) [3].

| Property | Value |
|-----------------|-------|
| M_p [kg] | 2 |
| δ [g/cc] | 8.96 |
| a [m] | 0.075 |
| U [km/s] | 2 |

Table 5: Impactor properties [7].

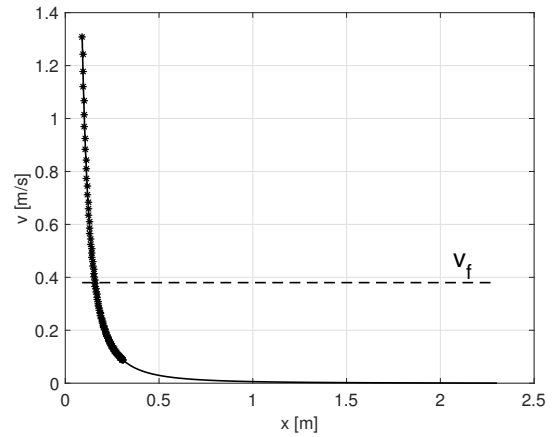


Fig. 14: Ejecta launch speed velocity as function of x , Eq. (29). The black star points are selected for the initial condition of the ejecta. The black dashed line represent the escape velocity, v_f , in Eq. (20).

6.3. Trajectory Evolution in the ACI, ACAF and Hill Reference Frames

In this section, the dynamics of the dust particles are shown in the ACI, ACAF and Hill frame. Figure 15 shows the distance of the dust from Ryugu asteroid over the time where the longest presence of 0.01 cm dust particles is, for this case, 25 hours. Figures 16-18 are the trajectories followed by dust particles of 0.01 cm in diameter after the reference impact event (red start in Figure 12). In those figures, 100 trajectories are selected having fixed one radial value (x coordinate equal to 0.16 m) and letting change the tangential angle (θ) to span the entire crater perimeter.

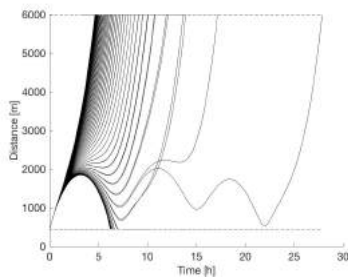


Fig. 15: Distance from the Ryugu asteroid surface.

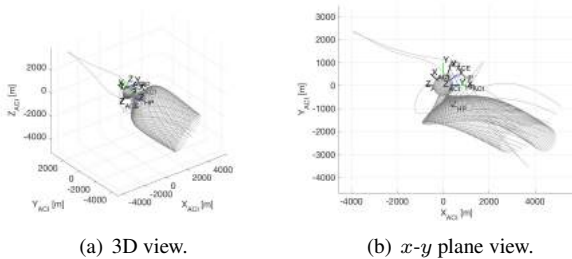


Fig. 16: ACI reference frame dust trajectories.

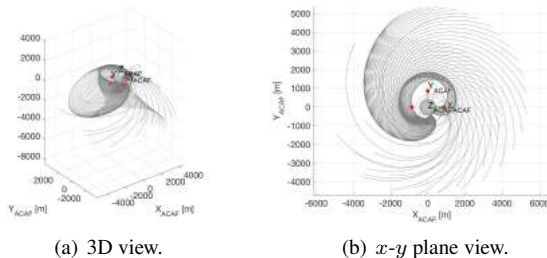


Fig. 17: ACAF reference frame dust trajectories.

Figure 19 shows the distance of the dust particles of size 0.01, 0.1, 1 and 10 cm from the asteroid surface for the reference impact (red star in Figure 12). With this numerical model, dust particle of 1 and 10 cm in size tend to have a slightly longer dynamics, however the region around the asteroid seems to be clear from dust particles after 30 hours.

Figure 20 shows the time of flight of the four size of dust particles as a function of the angle θ . As one can see, there is

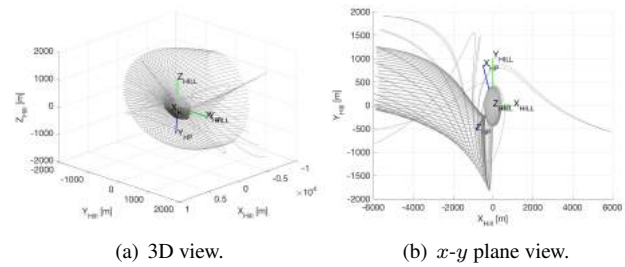


Fig. 18: Hill reference frame dust trajectories.

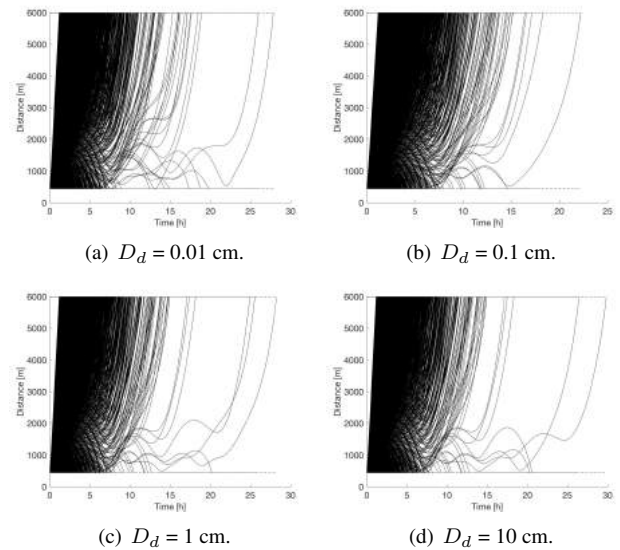


Fig. 19: Distance of the dust particles from the asteroid for the reference impact (red star in Figure 12).

an evolution of the picks. For very short Time of Flight (ToF) (less than 5 hours), the longest dynamics are close to 0° and 360° . The more the ToF increase the more the picks tends to shift closer to 180° . The maximum ToF seems to be close to 100° and 200° .

Figure 21 shows the TOF as function of the x and θ coordinates. These figures shows the x coordinate evolution as function of θ where the TOF of the four dust particles is the longest. Figures 22-23 show the maximum time of flight of dust particles in 0.01, 0.1, 1 and 1 cm size. Each points represents the maximum of the plots shown in Figure 21 as function of the coordinates x , in Figure 22, and of the coordinate θ , in Figure 23, respectively. For the impact points analysed, the region around the Ryugu asteroid seems cleared after a maximum or 40 hours.

Although this study shows that for the cases analysed there is no risk for Hayabusa 2 spacecraft after the SCI impact, further studies have to be carried out to finalise the stable regions around Ryugu and at which conditions on the asteroid surface particles can get there. A fully understanding of the dynamics around Ryugu with the asteroid shape model (polyhedron) is therefore necessary to have a high order precision of the dynamics close to the asteroid surface.

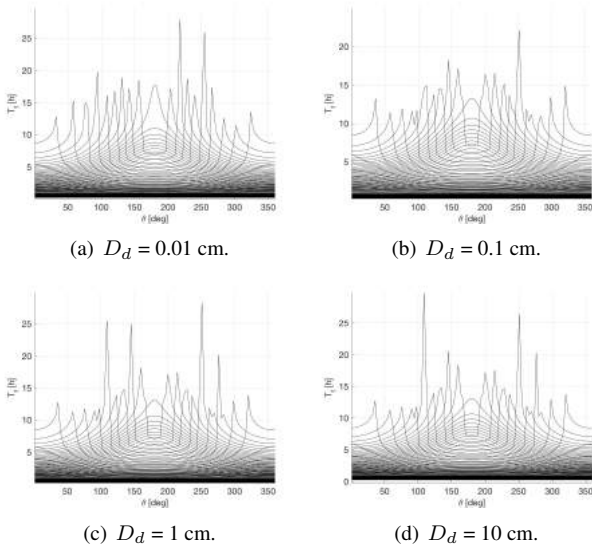


Fig. 20: Time of flight as function of the angle θ .

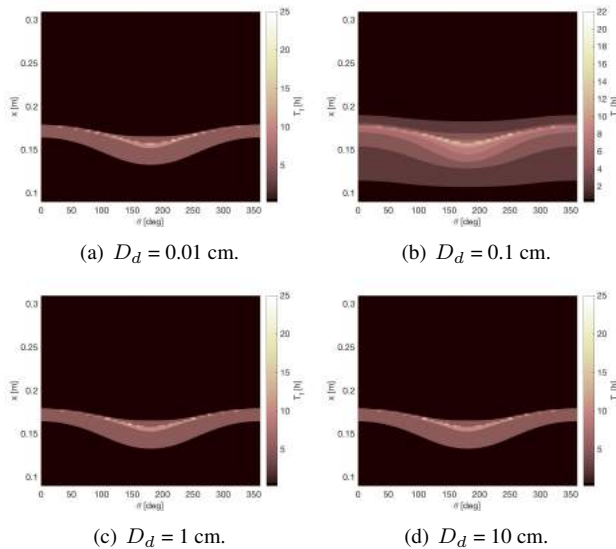


Fig. 21: Time of flight as a function of the x and θ coordinates.

7. Conclusions

In this paper, we assessed the hazard posed by Ryugu ejecta dynamics on Haybusa2 spacecraft. First, the dynamics close to the 1:1 resonances in the Asteroid-Centered Asteroid-Fix reference frame are investigated under the effect of the solar radiation pressure perturbation. When solar radiation pressure is taken into account, the dynamics cease to be autonomous, therefore dynamical substitutes of the equilibrium points seem to appear in their replacement. A numerical analysis was performed in the Asteroid-Centered Asteroid Inertial reference frame where the effect of solar radiation pressure and the Sun gravity was taken into account. Uncertainties in the impact point of the SCI and a model for the impact dynamics was used to initialise the motion of the ejecta from the launching site. For the cases analysed, the results show that 40 hours are enough to have particles of diameter size 0.01, 0.1, 1 and 10 cm in escape

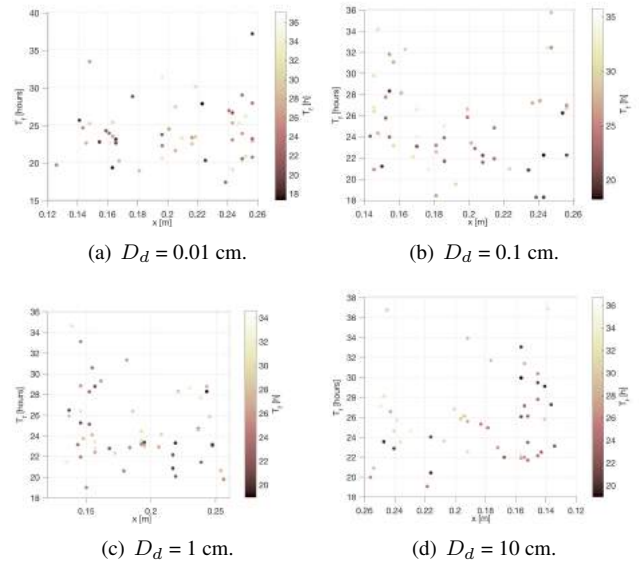


Fig. 22: Maximum time of flight for 51 impact points as function of the crater coordinate x .

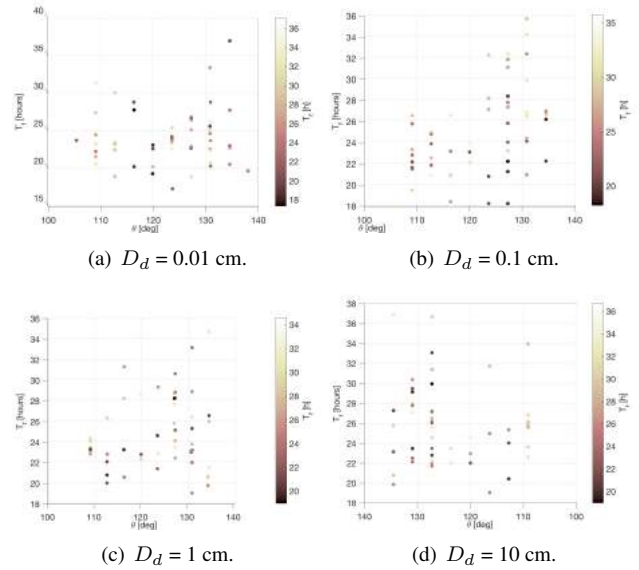


Fig. 23: Maximum time of flight for 51 impact points as function of the crater radial coordinate θ .

or re-impacting trajectory with the asteroid surface leaving the landing site cleared from potential debris.

Acknowledgments

This work was partially supported by JSPS KAKENHI Grant Number 26289325.

References

- [1] J. Bellerose and H. Yano. Dynamics of Asteroid 1999 JU3: target of the Hayabusa follow-on mission. *JSASS Aerospace Tech. Japan*, 8(ists27):Tk_23–Tk_28, 2010.

- [2] G Gómez, J. J. Masdemont, and J. M. Mondelo. *Libration Point Orbits and Applications: dynamical substitutes of the Libration points for simplified solar system models*. World Scientific Publishing Company., Singapore, 2003.
- [3] K. A. Holsapple and K. R. Housen. A crater and its ejecta: an interpretation of deep impact. *Icarus*, 187:345–356, 2007.
- [4] J. Matsumoto, T. Saiki, Y. Tsuda, and J. Kawaguchi. Numerical analysis of particle distribution with collisions around an asteroid. *Astrodynamics Symposium*, 2011.
- [5] P. Micheal, A. Cheng, M. Küppers, P. Pravec, J. Blum, M Delbo, S. F. Green, P. Rosenblatt, K. Tsiganis, J. B. Vincent, J. Biele, V. Ciarletti, A. hérique, S. Ulamec, I. Carnelli, A. Galvez, L. Benner, S. P Naidu, O. S. Barnouin, D. C. Richardson, A. Rivkin, P. Scherich, N. Moskovitz, A. Thirouin, S. R. Schwartz, C. A. Bagatin, and U. Yu. Science case for Asteroid Impact Mission (AIM): A component of the Asteroid Impact & Deflection Assessment (AIDA) mission. *Advances in Space Research*, 57:2529–2547, 2016.
- [6] J. M. Mondelo, S. B. Broschart, and B. F. Villac. Ballistic transfers across the 1:1 resonance around vesta following invariant manifolds. *Journal of Guidance and Control and Dynamics*, 36(4):1119–1133, 2013.
- [7] T. Saiki, H. Imamura, Y. Mimasu, and Y. Tsuda. Study on impact experiment of hayabusa 2 mission. *Proceedings of the AIAA/AAS Astrodynamics Specialist Conference, AAS 16-281*, 2016.
- [8] D. J. Scheeres. Orbit mechanism about asteroids and comets. *Journal of Guidance, Control and Dynamics*, 35(3):987–997, 2012. doi: 10.2514/1.57247.
- [9] D. J. Scheeres. *Orbital motion in strongly perturbed environment*. Springer., New York, 2012.
- [10] D.J. Scheeres. Dynamics about uniformly rotating triaxial ellipsoids: applications to asteroids. *ICARUS*, 110:225–238, 1994.
- [11] C. Snodgrass, C. Tubiana, J.-B. Vincent, H. Sierks, S. Hviid, R. Moissl, H. Boehnhardt, C. Barbieri, and et al. A collision in 2009 as the origin of the debris trail of asteroid P/2010 A2. *Nature*, 467:814–816, 2010. doi: 10.1038/nature09453.
- [12] Y. Tsuda, M. Yoshikawa, M. Abe, H. Minamino, and S. Nakazawa. System design of the Hayabusa 2 - Asteroid sample return mission to 1999 JU3. *Acta Astronautica*, 91:356–362, 2013.
- [13] D. A. Vallado. *Fundamentals of Astrodynamics and Applications, 4th edition*. Space Technology Library, 2013.
- [14] X Xin, D. J. Scheeres, and X. Hou. Forced periodic motions by solar radiation pressure around uniformly rotating asteroids. *Celest Mech Dyn Astr*, xx:xx, 2016. Doi:10.1007/s10569-016-9701-4.
- [15] Y. Yu, P. Michel, S. R. Schwartz, P. N. Shantanu, and A. M. B. Lance. Ejecta Cloud from a Kinetic Impact on the Secondary of a Binary Asteroid: I. Mechanical Environment and Dynamic Model. *arXiv:1603.07151v1 [astro-ph.EP]*, xx:xxx–xxx, 2016.